Two different transmission tunnels of light through double-layer gold nanohole arrays

2008 J. Phys.: Condens. Matter 20 415223

(http://iopscience.iop.org/0953-8984/20/41/415223)

IOP PUBLISHING JOURNAL OF PHYSICS: CONDENSED MATTER

J. Phys.: Condens. Matter **20** (2008) 415223 (6pp) doi:10.1088/0953-8984/20/41/415223

Two different transmission tunnels of light through double-layer gold nanohole arrays

Hongjian Li[1,2,4], **Suxia Xie**[1,2], **Renlong Zhou**[3], **Qiong Liu**[1], **Xin Zhou**[1,2] **and Min Yuan**[1]

[1] College of Physics Science and Technology, Central South University, Changsha 410083, People's Republic of China
[2] College of Materials Science and Engineering, Central South University, Changsha 410083, People's Republic of China
[3] College of Physics, Hunan University of Science and Technology, Xiangtan 411201, People's Republic of China

E-mail: lihj398@yahoo.com.cn

Received 26 July 2008
Published 18 September 2008
Online at stacks.iop.org/JPhysCM/20/415223

Abstract

We numerically simulate the enhancement of optical transmission through the double-layer gold nanohole arrays by using the finite-difference time-domain (FDTD) method. The optical transmission originates not only from the localized waveguide resonance but also from the well-recognized surface plasmon resonance due to the periodicity. The transmission characteristic of the two different resonance modes is also revealed clearly by analyzing the maps of electric field and electromagnetic energy distribution. In addition, we also show clearly the wave transport characteristics between the two-layer gold films.

(Some figures in this article are in colour only in the electronic version)

1. Introduction

The observation of extraordinary optical transmission (EOT) through periodic arrays of sub-wavelength holes in metallic films reported by Ebbesen *et al* [1] has launched a large number of experimental and theoretical studies. Many researchers demonstrated that the enhancement is attributed to the resonant coupling between the incident light and the surface plasmon excited on the metal–dielectric boundary of the periodic structure through evanescent waves [2–4]. The influence of the hole shapes on the transmission was investigated recently [5, 6]. It has been shown that the enhanced transmission phenomenon through hole arrays in perfect-conductor thin films may be attributed not only to the resonance-induced field enhancement arising from the periodic structure factor [7] but also the shape effect of the holes [7–11]. The similarities and differences between the structure factor resonance and general surface plasmon are investigated by Wen *et al* [12] and subsequently they discover that Fabry–Perot resonances and structure-factor-induced resonances are, in fact, the two limits of a single resonance phenomenon through a periodic array of sub-wavelength holes for electromagnetic waves. A recent explanation for the enhancement phenomenon is the collaboration of localized waveguide resonance with surface plasmon resonance [4, 8, 13, 14]. Work has been done mostly on the single-layer metal film with periodic hole arrays in the past few years, while studies of double-layer metal hole arrays have gained particular attention. Transmission for double-layer metal hole arrays with isotropic shapes (circular shapes) has been studied recently [15]. However, the mechanics for double-layer metal hole arrays with nonisotropic shapes has not been clearly explained.

In this paper, the enhanced normal transmission through the double-layer gold films perforated with periodic arrays of sub-wavelength rectangular holes is studied from two different resonance features: one is the localized waveguide resonance where each air hole can be considered as a truncated rectangle with both ends open to free space, while the other is the well-recognized surface plasmon resonance due to the periodicity of arrays. The normal electric field component E_z, tangential electric field component E_y and total energy distributions are shown in order to obtain a more detailed description (as shown in figures 4(a)–(c) and 5(a)–(c)). The positive and negative charge densities can extend to metal regions between

[4] Author to whom any correspondence should be addressed.

the holes. The periodic distribution of surface charges is consistent with the local charge dipole oscillations. The local charge dipole oscillation is revealed by the tangential electric field component (E_y) distribution [16]. We find that the tangential electric field component E_y and the total energy for a freestanding gold film nanohole array are nonzero only in the rectangular air hole region. The double-layer perforated gold films clearly show the energy transport of the two resonance peaks.

2. Theory

The three-dimensional (3D) FDTD method [17] is employed to simulate the interaction between the metal and the incident wave impinging on double-layer arrays of gold films structured with periodic sub-wavelength holes. The propagation of the light in the metal can be described by Maxwell's equations [17, 18]:

$$\begin{aligned} \frac{\mathrm{d}\vec{B}}{\mathrm{d}t} &= -\nabla \times \vec{E} - \vec{J}_B \qquad \vec{B} = \mu\vec{H}, \\ \frac{\mathrm{d}\vec{D}}{\mathrm{d}t} &= \nabla \times \vec{H} - \vec{J} \qquad \vec{D} = \varepsilon\vec{E}, \end{aligned} \tag{1}$$

where $\vec{D}$ is the displacement field, ε is the dielectric constant, $\vec{J}$ is the current density and $\vec{J}_B$ is the magnetic charge current density. $\vec{B}$ is the magnetic flux density (often called the magnetic field), while currently μ (the magnetic permeability) is specified as 1, so we do not need to distinguish between $\vec{B}$ and $\vec{H}$. Due to the frequency dependence of absorption and permittivity for a metallic material, we must consider the dispersion properties of the metal. With a Drude model, the frequency dependence can be described in our calculation in the following form [19]:

$$\varepsilon_m(\omega) = \varepsilon_\infty \left(1 - \frac{\omega_p^2}{\omega(\omega + \mathrm{i}\gamma)}\right) \tag{2}$$

where ε_0 is the permittivity of the vacuum, $\omega_p = 1.374 \times 10^{16}$ s^{-1} is the bulk plasma frequency of the gold, ω is the angular frequency of the incident wave and $\gamma = 4.08 \times 10^{13}$ s^{-1} represents the damping rate which characterizes the ohmic absorption loss. Physically, material dispersion arises because the polarization of the material does not respond instantaneously to an applied field E, and this is essentially the way that it is implemented in FDTD. In particular, $\vec{D} = \varepsilon\vec{E}$ is expanded to

$$\vec{D} = \varepsilon_\infty\vec{E} + \vec{P} \tag{3}$$

where ε_∞ is the instantaneous dielectric function (the finite-frequency response) and $\vec{P}$ is the polarization density in the material. $\vec{P}$, in turn, has its own time-evolution equation, and the exact form of this equation determines the frequency dependence $\varepsilon(\omega)$. In particular, any material dispersion of the form of a sum of harmonic resonances can be given by

$$\varepsilon(\omega, \mathrm{X}) = \varepsilon_\infty(\mathrm{X}) + \sum_n \frac{\sigma(\mathrm{X}) \cdot \omega_n \Delta\varepsilon_n}{\omega_n^2 - \omega^2 - \mathrm{i}\omega\gamma_n} \tag{4}$$

where ω_n, γ_n and $\Delta\varepsilon_n$ are user-specified constants, and $\sigma(\mathrm{X})$ is a user-specified function of position (usually 0 or 1). This corresponds to evolving $\vec{P}$ via the equations

$$\vec{P} = \sum_n \vec{P}_n \tag{5}$$

$$\frac{\mathrm{d}^2\vec{P}_n}{\mathrm{d}t^2} + \gamma_n\frac{\mathrm{d}\vec{P}_n}{\mathrm{d}t} + \omega_n^2\vec{P}_n = \sigma_n(\mathrm{X})\omega_n^2\Delta\varepsilon_n\vec{E}. \tag{6}$$

That is, we must store and evolve a set of auxiliary fields $\vec{P}_n$ along with the electric field in order to keep track of the polarization $\vec{P}$. Essentially any $\varepsilon(\omega)$ could be modeled by including enough of these polarization fields. To implement a Drude model of $\varepsilon(\omega)$, in which ω_n is zero in the denominator, we just set ω_n to be a very small number (e.g. 1×10^{-20}) and make $\Delta\varepsilon_n$ large to compensate in the numerator, where γ, ω_0 and $\Delta\varepsilon$ are material parameters. The energy loss due to the absorption by this resonance is simply

$$\Delta U = \vec{P}\frac{\mathrm{d}\vec{E}}{\mathrm{d}t}. \tag{7}$$

When a plane wave is incident on the double-layer metal films with periodic hole arrays, the surface plasmon enhances the energy transmission. The interaction between light and the surface plasmon obeys momentum conservation [1]:

$$\vec{k}_{\mathrm{sp}} = \vec{k}_0 \sin\theta \pm m\vec{u}_x \pm n\vec{u}_y, \tag{8}$$

where $\vec{k}_0 \sin\theta$ is the in-plane component of the wavevector of the incident light, $k_0 = w/c$. $\vec{u}_x$ and $\vec{u}_y$ are the reciprocal lattice vectors, $|\vec{u}_x| = |\vec{u}_y| = 2\pi/a_0$, and m and n are integers expressing the mode indices. From the conservation of energy, the surface plasmon vector $\vec{k}_{\mathrm{sp}}$ on a metallic film can be found [20]:

$$|\vec{k}_{\mathrm{sp}}| = |\vec{k}_0|\sqrt{\frac{\varepsilon_1\varepsilon_2}{\varepsilon_1 + \varepsilon_2}} \tag{9}$$

where ε_1 and ε_2 are the dielectric constants of the incident medium (air here) and the metal films. For the normal incidence, from equation (8) with $\theta = 0$ associated with equation (9), the wavelengths of the exited surface plasmon resonance modes are given approximately by $\lambda_{\max}$ as follows [1]:

$$\lambda_{\max}(m, n) \cong \frac{a_0}{\sqrt{m^2 + n^2}}\sqrt{\frac{\varepsilon_1\varepsilon_2}{\varepsilon_1 + \varepsilon_2}}. \tag{10}$$

In addition, theoretically, a rectangular waveguide with perfect metal walls has the resonant frequencies given by

$$\omega = \frac{\pi}{\sqrt{\mu\varepsilon}}\sqrt{\frac{m}{b_x} + \frac{n}{b_y}} \tag{11}$$

where integers m and n denote the number of half-wave variations in the x and y directions, respectively. b_x and b_y denote the x and y dimensions of the waveguide, respectively.

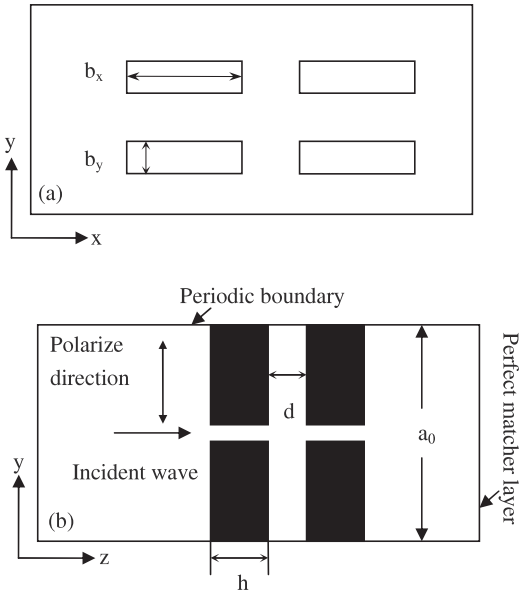

Figure 1. Schematic illustration of the double-layer metal hole arrays structure. (a) Top view of the structure: the rectangular air holes of sides b_x and b_y are perforated on a freestanding gold film of thickness h for each layer. (b) yz cross section of the computational domain consisting of a single unit cell of the double-layer hole arrays. A normal incident light wave polarized along the y direction illuminates the array along the z direction. Periodic boundary conditions are imposed on the four surfaces perpendicular to the gold film, while perfect matched layers are imposed at the left and right surfaces.

3. Results and discussion

Two infinite arrays of sides $b_x = 0.792a$ and $b_y = 0.176a$ rectangular apertures perforated on two freestanding gold films of thickness $h = 0.427a$ are shown schematically in figure 1(a), where $a = 750$ nm. In addition, the lattice constant is $a_0 = a$. The layer spacing is fixed at $d = 0.29a$. In figure 1(b), we can see the input light wave is polarized along the short edge of the coaxial rectangular holes (the y direction) and propagated to the two gold films' surface along the z direction. In addition, periodic boundary conditions are imposed on the four surfaces in the holes perpendicular to every gold film. Perfect matched layers are imposed at the left and right surfaces of each layer.

Figure 2 shows the normalized transmission spectrum for a single-layer gold hole array (the solid line) and double-layer gold hole arrays (the dot line) at normal incidence. In the single-layer gold hole array transmission spectrum, the transmission peaks are observed at 0.935 μm with a transmission of 0.861, and at 1.499 μm with a transmission of 0.776. The anomalous transmissions mean that not only the electromagnetic energy impinging directly on the holes gets transmitted but also part of the energy shining on the gold surface is converted into transmission, and such transmission peaks are attributed to the surface plasmon at the metal–air interface. In the transmission spectrum for the double-layer gold hole arrays, we obtain two transmission peaks at the same location as that of the single-layer hole array but with much

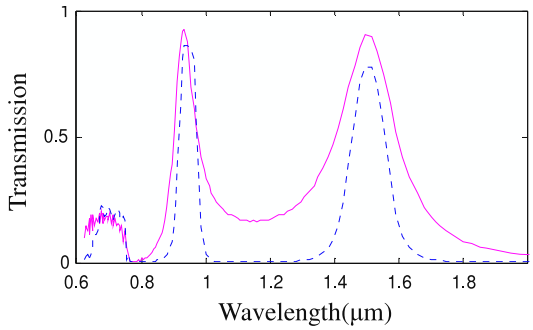

Figure 2. The normalized transmittances for the single-layer metal hole array (the solid line) and the double-layer metal hole arrays (the dotted line).

narrower peak widths. The quality factor of the transmission peaks, which can be defined as $Q = \lambda_0/\Delta\lambda$, increases when the number of building blocks is increased, where λ_0 is the wavelength of the peak and $\Delta\lambda$ is the half-width of the peak. For the two transmission peaks with 0.935 and 1.499 μm peak wavelengths, the Q values are $Q = 11.308$ and 5.5173, respectively, for the single-layer gold hole array, while $Q = 15.560$ and 14.450, respectively, for the double-layer gold hole arrays. The intensity of transmission peaks decreases when the number of gold layers is increased from one to two. However, the values are still extraordinary. These features may originate from multiple scatterings and the coupling of electromagnetic waves in the double-layer films. More interestingly, from both transmission spectra in figure 2 one can find the cutoff wavelength region around 750 nm corresponding to Wood's anomaly which should occur at wavelength $\lambda = a_0$. Two transmission peaks of enhanced transmission appear above the cutoff wavelength range. In addition, in the double-layer hole arrays transmission spectrum, it can be seen that the cutoff wavelength region around 750 nm becomes wider, extending to a longer wavelength. Furthermore, in a wide wavelength region between the two resonant peaks, no light wave can transmit; similarly, almost no light wave can transmit at a wavelength longer than the second peak position. It is intriguing in designing devices such as good-performance, band-pass metal filters.

We also studied three structures with different lattice constants (a) $a_0 = 0.9a$, (b) $a_0 = 0.95a$ and (c) $a_0 = 1.0a$, respectively. The calculation results are shown in figure 3. The lattice constant a_0 increases while the hole size is fixed. The long-wavelength peak does not change significantly while the short-wavelength peak is redshifted obviously. The transmissions are still very high and increasing as the lattice constant increases. Another interesting phenomenon is that the transmission bandwidths of the two resonances are quite different. The long-wavelength transmission resonance wavelength width is always wider than that of the short-wavelength one.

Now we discuss the mechanism of such an anomalous transmission property for the double-layer gold hole arrays. In the visible region, the localized surface plasmon located close to the gold surface attenuates exponentially with distance on the metal surface. When the two layers of the gold hole arrays

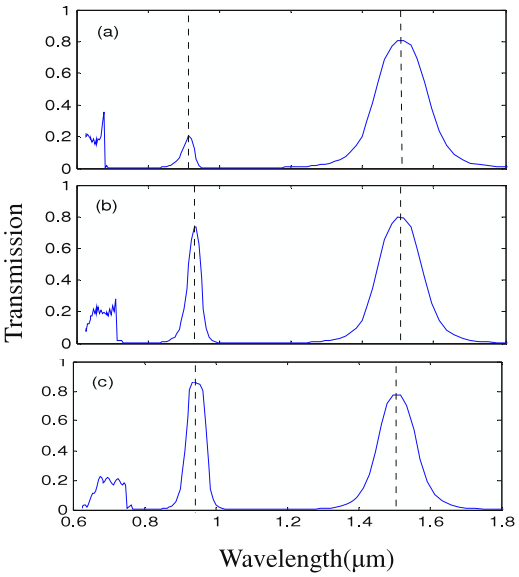

Figure 3. (a) Normalized transmission for the double-layer metal hole arrays with a square array of rectangular $b_x \times b_y$ holes for different lattice constants: (a) $a_0 = 0.9a$, (b) $a_0 = 0.95a$ and (c) $a_0 = 1.0a$. The thickness of each film is 320 nm.

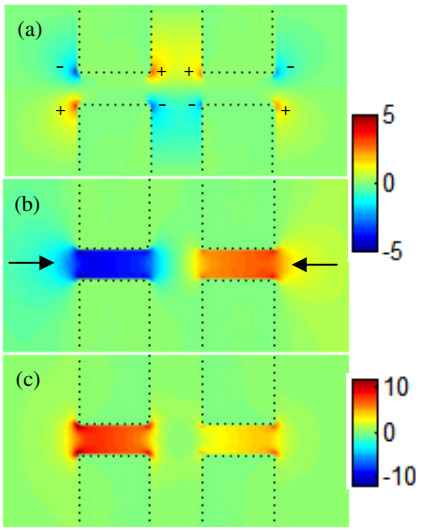

Figure 4. yz cross section for the amplitude evaluated at the resonant wavelength 1.499 μm of (a) the normal electric field component E_z distribution, (b) the tangential electric field component E_y distribution and (c) the total energy distribution of magnetic and electric fields.

are placed close together, the surface plasmons excited on these layers couple with each other. Consequently, a change of the transmission spectrum is expected. To investigate the validity of the physical picture in the infrared region, we simulated the electric field distribution and the total energy distribution of the double-layer gold hole arrays using the FDTD method. Figures 4(a) and (b) show the normal electric field components E_z and tangential electric field components E_y at wavelength 1.499 μm for the double-layer hole arrays in the y–z plane, respectively. From figure 4(a) we can find that the normal

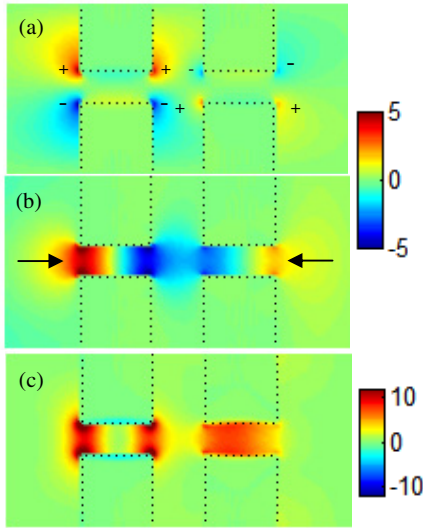

Figure 5. yz cross section for the amplitude evaluated at the resonant wavelength 0.935 μm of (a) the normal electric field component E_z distribution, (b) the tangential electric field component E_y distribution and (c) the total energy distribution of magnetic and electric fields.

electric field component E_z is seen to be concentrated around the metal region along the long edges of the rectangular hole. According to the boundary condition $\vec{n} \cdot \vec{E} = \sigma/\varepsilon_0$, where σ is the surface charge density. Moreover, in the normal direction, $\vec{n} = n\vec{z}$. Therefore we are able to determine the magnitude of surface charges through detecting $|E_Z|$. The positive and negative charge densities (labeled with $+$ and $-$) as measured by the normal electric field E_z can extend to the metal regions between the holes [16] and we also can see the charges tend to accumulate at the metal corners. Furthermore, the charge patterns on the two surfaces are nearly the same for each layer, but they have opposite signs. Additionally signs at the output side of the first layer are the same as that at the input side of the second layer. From figure 4(a) we obtain a periodic distribution of surface charges and such a distribution is consistent with the local charge dipole oscillation in the direction perpendicular to the long edges of the rectangular air holes. Seemingly, these 'dipoles' are flanked by opposite surface charges and these periodic charges establish a standing wave resonance in the rectangular air hole region for both layers. The local charge dipole oscillation is also revealed from the tangential electric field component E_y that is mostly concentrated in the hole region decaying exponentially with distance of the metal–air interface along the $-z$ and z directions (as shown in figure 4(b)). E_y inside holes of the first layer is negative, which is the opposite to that inside holes of the second layer. The resonance mode at wavelength 1.499 μm can be explained by the localized waveguide resonance. Each air hole in the films can be considered as a truncated rectangular waveguide with four metal walls and two sides open to free space. The truncated waveguide forms a low-quality resonator. It is dependent on the hole shape but almost independent of the period of the structure [19]. Additionally, even if the gold film is very thin the waveguide resonances exist, which can be expressed by the Fabry–Perot effect [8, 12].

The total energy distribution of the electric and the magnetic field are obtained in the yz plane as shown in figure 4(c). It can be clearly seen in figure 4(c) that the total energy is mostly concentrated inside the holes for both layers. It seems the total energy distribution for the second layer is smaller than that for the first layer, which may due to the multiple scatterings in the two layers. The localized waveguide resonance mode transports from the first layer to the second layer through the air gap with self-guiding behavior.

The electric fields and total energy distributions of the near-field at the peak transmission wavelength 0.935 μm is also shown, which can help us to understand how the light passes through the holes. The enhanced transmittance is due to the well-recognized structure-factor-induced resonance determined by the periodicity. Figures 5(a)–(c) show the normal electric field components E_z, the tangential electric field components E_y and the total energy distribution of the calculation results for electromagnetic waves at wavelength 0.935 μm for the double-layer metal hole arrays in the y–z plane, respectively. As is known [7, 8] the surface plasmon mode originates from the well-recognized surface plasmon structure-factor-induced resonance effect. The positive and negative charge densities (labeled with + and −) as measured by the normal electric field E_z can extend to the metal regions between the holes in figure 5(a). As can be seen the signs of charge densities at one long edge of the rectangular hole are opposite to those at the other long edge for every metal–air interface, which is similar to that of figure 4(a). However, for each layer, charge density signs at the input side and the output side are the same. Coupling of the surface charges at the region between the two layers can be observed. Additionally, the E_z intensity at the input side of the double-layer arrays is larger than that at the output side. We obtained a periodic distribution of surface charges (labeled with + and −) and such a distribution is consistent with the local charge dipole oscillations that establish a standing wave resonance (labeled with → and ←) along the y direction inside the rectangular air holes for both layers. The local charge dipole oscillation is also revealed from the tangential electric field component E_y. For the first layer, E_y is positive inside the holes near the entrance interface, while it is negative at the exit side. Instructive coupling of the surface plasmon with different signs is expected. The electromagnetic energy simulated result shown in figure 5(c) is that the total energy is mostly located around both ends of each hole for the first layer. However, for the second layer, energy is concentrated inside the hole region. As a result, the wave can propagate from the first film to the second film due to the surface plasmon resonance, which is different from the self-guiding effect for the waveguide resonance.

Generally speaking, the surface plasmon is generated from the interaction between the surface charge oscillation and the electromagnetic field of the light. It is mainly a longitudinal, compressive electronic density wave, propagating along the metal surface (the y direction) following a certain dispersion [21, 22]. The surface plasmon resonance coupling light into and out of the holes enhances the field at two ends of each hole in the double-layer gold hole arrays. Therefore, the surface plasmon resonance plays an important role in transmission enhancement through the sub-wavelength hole arrays. Additionally, in this paper, we observe that the surface plasmon (E_y) is mostly concentrated inside the holes, which is different from the general surface plasmon.

4. Conclusions

In conclusion, we have investigated the optical transmission properties of the double-layer gold nanohole arrays. We have clearly shown the two different resonance tunnels by using double-layer gold nanohole arrays. The mechanism of the transmission is mainly attributed to two reasons as follows: one is the localized waveguide resonance and the other is the surface plasmon resonance. The corresponding field distributions and energy distributions are also presented for a better understanding of how the light wave passes through the holes. When light transmits from one metal–film nanohole array to another, the energy transporting behaviors of the two resonance modes are different: one is light self-guiding transport behavior through the air gap, while the other one is dipole oscillation transporting behavior through the air gap. The good band-pass transmission property can be applied in device designs such as a metal filter.

Acknowledgments

This work was funded by the National Natural Science Foundation of China under grant no. 60708014, the Distinguished Youth Foundation of Hunan Province under grant no. 03JJY1008, the Science Foundation for Post-doctorate of China under grant no. 2004035083, and the Natural Science Foundation of Hunan Province under grant no. 06JJ20034.

References

[1] Ebbesen T W, Lezec H J, Ghaemi H, Thio T and Wolf P A 1998 *Nature* **391** 667
Ghaemi H F, Thio T, Grupp D E, Ebbesen T W and Lezec H J 1998 *Phys. Rev.* B **58** 6779
William L B, Alain D and Ebbesen T W 2003 *Nature* **424** 824
[2] Barnes W L, Murray W A, Dintinger J, Devaux E and Ebbesen T W 2004 *Phys. Rev. Lett.* **92** 107401
[3] Garca-Vidal F J, Lezec H J, Ebbesen T W and Martín-Moreno L 2003 *Phys. Rev. Lett.* **90** 213901
Martín-Moreno L, Garcia-Vidal F J, Lezec H J, Pellerin K M, Thio T, Pendry J B and Ebbesen T W 2001 *Phys. Rev. Lett.* **86** 1114
[4] Tang Z H, Peng R W, Wang Z, Wu X, Bao Y J, Wang Q J, Zhang Z J, Sun W H and Wang M 2007 *Phys. Rev.* B **76** 195405
[5] van der Molen K L, Klein Koerkamp K J, Enoch S, Segerink F B, van Hulst N F and Kuipers L 2005 *Phys. Rev.* B **72** 045421
[6] Degiron A and Ebbesen T W 2005 *J. Opt. A: Pure Appl. Opt.* **7** S90
[7] Beruete M, Sorolla M, Campillo I, Dolado J, Martin-Moreno L, Bravo-Abad J and Garcia-Vidal F J 2005 *IEEE Trans. Antennas Propag.* **53** 1897
[8] Ruan Z C and Qiu M 2006 *Phys. Rev. Lett.* **96** 233901

[9] Mary A, Sergio G Rodrigo, Martín-Moreno L and García-Vidal F J 2007 *Phys. Rev.* B **76** 195414
[10] Garcia-Vidal F J, Moreno E, Porto J A and Martin-Moreno L 2005 *Phys. Rev. Lett.* **95** 103901
Garcia-Vidal F J, Martin-Moreno L, Moreno E, Kumar L K S and Gordon R 2006 *Phys. Rev.* B **74** 153411
[11] Strelniker Y M 2007 *Phys. Rev.* B **76** 085409
[12] Hou B, Hang Z H, Wen W J, Chan C T and Sheng P 2006 *Appl. Phys. Lett.* **89** 131917
Hou B, Mei J, Ke M Z, Wen W J, Liu Z Y, Shi J and Sheng P 2007 *Phys. Rev.* B **76** 054303
[13] Chen Y G, Wang Y H, Zhang Y and Liu S T 2007 *Opt. Commun.* **274** 236–40
[14] Zhou R L, Chen X S, Wang S W, Lu W, Zeng Y, Chen H B, Li H J, Xia H and Wang L L 2008 *Solid State Commun.* **145** 23
[15] Miyamaru F and Hangyo M 2005 *Phys. Rev.* B **71** 165408
[16] Cao H and Nahata A 2004 *Opt. Express* **12** 3664
[17] Taflove A 2000 *Computational Electrodynamics: the Finite-Difference Time-Domain Method* 2nd edn (Boston, MA: Artech House Publishers)
[18] Muller R, Malyarchuk V and Lienau C 2003 *Phys. Rev.* B **68** 205415
[19] Palik E D 1991 *Handbook of Optical Constants in Solids* vol 1 (New York: Academic)
[20] Raether H 1988 *Surface Plasmons on Smooth and Rough Surfaces and on Gratings* (Berlin: Springer)
[21] Altewischer E, Van Exter M P and Woerdman J P 2002 *Nature* **418** 304
[22] Hecht B, Bielefeldt H, Novotny L, Inouye Y and Pohl D W 1996 *Phys. Rev. Lett.* **77** 1889